Engineering Fracture Mechanics 215 (2019) 193–210

Contents lists available at ScienceDirect

Engineering Fracture Mechanics

journal homepage: www.elsevier.com/locate/engfracmech

Critical comparison of the boundary effect model with cohesive crack model and size effect law

Christian Carloni[a], Gianluca Cusatis[b], Marco Salviato[c,*], Jia-Liang Le[d], Christian G. Hoover[e], Zdeněk P. Bažant[f]

[a] Chair, ACI Committee 446, Fracture Mechanics; and Associate Professor, Civil and Environmental Engineering, Case Western Reserve University, Cleveland, Ohio, 44106, USA
[b] Past Chair, ACI Committee 446, Fracture Mechanics; and Associate Professor, Civil and Environmental Engineering, Northwestern University, Evanston, Illinois, 60208, USA
[c] Assistant Professor, William E. Boeing Department of Aeronautics and Astronautics, University of Washington, Seattle, Washington 98195-2400, USA
[d] Associate Professor, Civil, Environmental, and Geo- Engineering, University of Minnesota, Minneapolis, Minnesota, 55455, USA
[e] Assistant Professor, School of Sustainable Engineering and the Built Environment, Arizona State University, Tempe, Arizona, 85281, USA
[f] McCormick Institute Professor and W.P. Murphy Professor of Civil and Mechanical Engineering and Materials Science, Northwestern University, Evanston, Illinois, 60208, USA

ARTICLE INFO

Keywords:
Quasibrittle materials
Concrete structures
Fracture mechanics
Energetic size effect
Size effect law
Statistical size effect
Size effect justification
Analysis of experimental data
Design codes

ABSTRACT

For several decades it has been clear that the size effect on structural strength, exhibiting a major non-statistical component, is a quintessential property of all quasibrittle materials. However, progress in design codes and practice for these materials has been retarded by protracted controversies about the proper mathematical form and justification of the size effect law (SEL). A fresh exception is the American Concrete Institute which, in 2019, becomes the first concrete code-making society to adopt the SEL based on quasibrittle fracture mechanics. This article begins by discussing several long-running controversies that have recently abated, and then focuses critically on the so-called Boundary Effect Model (BEM), promoted for concrete relentlessly for two decades, in ever-changing versions, by Xiaozhi Hu et al. The BEM is here compared to the quasibrittle SEL based on asymptotic matching. Its errors, weaknesses and inconsistencies are identified—including incorrect large- and small-size asymptotic size effects, conflicts with broad-range comprehensive test data and with the cohesive crack model, incorrect aggregate-size dependence of strength, illogical dependence on ligament stress profile, inability to capture the statistical part of size effect at large sizes, simplistic effect of boundary proximity, and lack of distinction between Type 1 and 2 size effects. In contrast to the SEL, the BEM is not applicable to mixed and shear fracture modes and to complex geometries of engineering structures, and is not transplantable from concrete to other quasibrittle materials.

The purpose of this critique is to help crystallize a consensus about the proper size effect formulation, not only for concrete structures but also, and mainly, for other quasibrittle materials and structures, including airframes made of fiber composites, ceramic components and micrometer-scale devices, and for failure assessments of sea ice, rock, stiff soils, bone, and various bio- or bio-mimetic materials, for all of which the non-statistical size effect is yet to be widely accepted in practice.

* Corresponding author.
E-mail address: salviato@aa.washington.edu (M. Salviato).

https://doi.org/10.1016/j.engfracmech.2019.04.036
Received 1 February 2019; Received in revised form 15 April 2019; Accepted 28 April 2019
Available online 08 May 2019
0013-7944/ © 2019 Elsevier Ltd. All rights reserved.

1. Introduction to problem faced

The scaling is a fundamental property of every physical theory—if it is not understood, the theory itself is not understood. For elastic and elasto-plastic structures, this dictum has required no attention because their scaling law is trivial—the size effect on structural strength is nil (except for Weibull statistical size effect, which is not discussed here). However, the situation changed with the emergence in 1984 of the energetic size effect law (SEL) for quasibrittle failure [1,2], for which correct size effect predictions necessitate the theories of quasibrittle or cohesive fracture, and of damage mechanics. For such theories, exact analytical solutions are not feasible.

So the objective has been to find an accurate enough model capturing the transition between the simple power laws that characterize the opposite asymptotic behaviors. This has been a challenge that has led to extensive polemics and, unfortunately, persistent controversies. One controversy, which has been particularly persistent, is the subject of this comparative study.

2. Progress-retarding controversies to be overcome

As a result of experiments begun in the 1970s, the importance of size effect for concrete and other quasibrittle materials for structural design codes has been recognized [3–8]. The introduction in the 1980s of Weibull statistical power-law size effect [9–12] into the shear specifications of the design code of the Japan Society of Civil Engineers (JSCE) [13] was a pioneering act for those times. Later, though, it transpired that the Weibull's statistical power-law size effect, still embedded in the JSCE specifications [13], is not correct for their intended purpose since a dominant large crack grows stably before failure at a specific location dictated by mechanics.

In the American Concrete Institute (ACI), design code changes depend on democratic voting of large committees dominated by cautious practitioners, who insist on broad verification and broad consensus. Inevitably, change is slow and requires protracted discussions. After discussions lasting for more than three decades, and thanks partly to the efforts of ACI Committee 446, Fracture Mechanics (chaired currently by the first author, C.C., and previously by the second author, G.C.), which approved the SE in 2007 (unanimously, under K. Gerstle chairmanship) [90], a consensus has finally crystallized in the ACI. The result is that the SEL has been approved for the shear of beams and punching shear of slabs, and for the compression struts of the strut-and-tie model and is now incorporated into the 2019 update of the ACI design code, ACI Standard 318. The cautiousness saved ACI from enacting anything wrong. The ACI thus becomes the first code-making society that implicitly accepts the quasibrittle fracture mechanics as a basis of the code.

The long delay has largely been caused by persistent controversies about alternative theories of size effect. An early controversial idea, advanced in 1993, claimed that the size effect in concrete fracture was caused by the fractal nature of concrete microstructure and its fracture surfaces. This controversy has abated after the critique, discussion and rebuttal in [14,15], and seems no longer to hinder progress in design codes.

The European *fib* Model Code 2010 [16] has also included a size effect for shear failures in their specifications. But its derivation is simplistic and, from the mechanics viewpoint, not justified. It is based on a controversial notion, surviving for almost three decades [18,22,23,26], namely that the size effect in shear failures of reinforced concrete beams is somehow governed by the longitudinal strain [23] or by the width of the dominant shear crack. This latter crack itself is imagined to be governed by the longitudinal strain or by spacing of parallel shear cracks as they form at about one half of the failure load [22]. This hypothetical empirical approach has not received traction in ACI. But it made its way into the current European concrete design code [16]. A variant [17–29] is now proposed for the 2020 European concrete design code (Model Code 2020), but faces serious criticism [30].

This proposed Model Code version was modified so as to give a size effect curve similar to SEL [23]. It estimates the crack width from the longitudinal strain of concrete calculated for a certain point by the beam bending theory with plane cross sections remaining plane [30, c.f.]. However, 14% differences from the SEL exist. The derivation, based on beam mechanics with plane cross sections, is simplistic, illogical and misleading to students trying to understand the cause of size effect. In ACI, though, this approach received no traction.

On the other hand, another old controversy, initiated in 2000 by an article of Hu and Wittmann [31], still goes on unabated and generates doubts. In this article, Hu and Wittmann proposed to explain and model the size effect by the so-called Boundary Effect Model (BEM), not to be confused with the Boundary Element Method used for the solution of boundary value problems in mechanics [32, e.g]. Subsequently, various versions of BEM and critiques of the competing model were iterated in about twenty papers by Xiaozhi Hu et al. [33–36, e.g.], culminating in 2017 with [37]. In response to previous criticisms [39,40], Hu et al. modified their BEM empirically again and again, but without abandoning its faulty original premise (to be explained here) [31,33–37]. Hu et al. repeatedly claim [31,33–37, e.g.] that the size effect in reinforced concrete is caused by a boundary layer consisting of aggregates whose finite size causes different properties. Such a layer, of course, exists, but is automatically taken into account through the finiteness of the representative volume element (RVE) of the material and of the fracture process zone (FPZ). But the main size effect source in cohesive fracture mechanics is the release of stored energy during stable growth of a crack with a finite fracture process zone (FPZ), and the associated stress redistribution, which is ignored by the BEM.

In their last critique of SEL, Hu et al. [37] cited and used the comprehensive concrete fracture experiments of Hoover et al. [41,42] at Northwestern University, which explored a very broad size range (1: 12.5) and notch lengths (0 to 30% of cross section), and had an exceptionally low coefficient of variation of regression errors (only 2%), thanks partly to casting all the specimens from one and the same batch of concrete.

However, Hu et al. [37] did not cite and use Hoover et al.'s subsequent analysis of these tests in [43]. This analysis showed

excellent agreement with the SEL and with cohesive fracture mechanics in general, and allowed calibrating the shape of the cohesive softening stress-displacement relation with a size-independent fracture energy. In fact, the motivation for Hoover et al.'s meticulously conducted tests was to disprove the hypotheses of the BEM, as explained in what follows. Hu et al. further ignored the subsequent article [38] which demonstrated an excellent agreement of an asymptotic-matching formulation with Hoover et al.'s test data.

By contrast, Hu et al. [37] did cite the subsequent tests by Siddık Şener et al. [44] at Gazi University in Ankara. These were near-duplicates of Hoover et al.'s tests. But they were smaller in scope and exhibited such a high scatter that any differences among the size effect theories could hardly be discerned. The scatter of the data in Şener's article [44] is, in fact, so high that it prevents disproving BEM.

Although the BEM controversy eventually failed to prevent the adoption of the SEL by the ACI, it doubtless still rests on the mind of some members of concrete code committees in Europe and Asia, as well as all the designers of large concrete structures afflicted by size effect. Any whiff of controversy tends to retard modernization of the design practice and codes. Thus, it is important to clarify the deficiencies of BEM by rigorous mathematical arguments based on fracture mechanics, which is the objective of this article.

In contrast to the American concrete research community, in which the size effect law based on cohesive fracture mechanics has by now become a consensus, the worldwide research and engineering communities dealing with other quasibrittle materials have not yet accepted the energetic size effect of cohesive fracture mechanics. They still regard the Weibull statistics [10–12] as the only source of size effect, even though this effect is, in reinforced concrete shear failures, either nonexistent or only a negligible contributor.

In particular, this is the situation for other quasibrittle materials including polymer-fiber composites, tough or toughened ceramics, sea ice, many rocks, landslides, bio-materials (e.g., bone), nano-composites, polysilicon and micrometer scale devices [1,2,12,40,45–51,53–73]. For structures made of these materials, the size range from lab specimens to engineering applications often spans several orders of magnitude. As a notable example, one can think of the scaling of structural strength from composite coupons featuring gauge lengths of few hundreds of millimeters to the composite wing of an aircraft such as the Boeing 787 characterized by a span of many meters. Another example is the scaling of structural strength from lab specimens of few millimeters to microdevices such as MEMS or electronic circuits featuring characteristic lengths on the order of microns.

Young researchers entering these fields are inevitably getting confused by seeing competing theories, such as the BEM. For them, rigorous and experimentally supported explanation has thus become critically important. The size effect problem was tackled first for concrete because many civil engineering structures are far larger than any feasible tests, and because the fracture process zone length, about 1 ft., manifests itself clearly in normal laboratory tests. However, in view of the aforementioned dictum, the size effect is, aside from concrete, equally important for all quasibrittle materials. Casting doubt on the size effect theory for concrete confuses engineers dealing with the size effect in any of these materials.

3. Review of Type 1 and 2 size effect laws: Theoretical Background

Due to the complex mesostructure, the fracturing process of quasibrittle materials (such as concrete, ceramics, rocks, rigid foams, fiber composites, wood sea ice, stiff soils, consolidated snow and many bio-materials) generally features a significant stress redistribution. This phenomenon, which is typically characterized by the emergence of a non-linear fracture process zone (FPZ), leads to a deterministic size effect in structures weakened, prior to maximum load, by stably grown large cracks, or by notches. This type of size effect is generally referred to as *Type 2 size effect* [1,2,45–51].

In the case of quasibrittle structures of positive geometry [50], failing at crack initiation from a smooth surface, the size effect is caused by a combination of stress redistribution in the FPZ with strength randomness. In fact, because of the material heterogeneity, a finite FPZ must develop before the cracking can coalesce into a macrocrack of finite length emanating from the surface. At the same time, the location of crack initiation will depend on the spatial random distribution of material strength. This type of energetic-statistical size effect is generally referred to as *Type 1 size effect* [12,51,53,54,56,57,60,62–64,74].

The following sections aim at providing a brief overview of Type 1 and 2 size effect laws and their physical foundations. The interested reader can find a more comprehensive description in the abundant literature produced on this topic in the past four decades [1,2,12,40,45–71,73].

3.1. Size effect in structures featuring large cracks or notches (Type 2 size effect)

In quasibrittle structures, the size of the non-linear FPZ occurring in the presence of a large stress-free crack is usually not negligible [1,46–48,50,65,69–71,73]. The stress field along the FPZ is nonuniform and decreases with crack opening, due to discontinuous cracking, crack deflection, and frictional pullout of grains or inhomogeneities. In this scenario, the theories such as Linear Elastic Fracture Mechanics (LEFM) fail to capture the Type 2 size effect, since they inherently assume the FPZ to be negligible and hence lack a characteristic length representing the fracturing process.

This deficiency can be overcome by equipping LEFM with a fracture length scale by means of the simple approach of equivalent linear elastic fracture mechanics (LEFM). According to this approach, the elastic crack is extended by distance r_1 so that the resultant of the stress field induced by the equivalent crack (area EBCD in Fig. 1) matches the resultant of the cohesive stresses in the FPZ (area OBCO in Fig. 1). According to the Saint-Venant principle, the stress field sufficiently far from the tip is equivalent to the one induced by the FPZ. Accordingly, the equivalent approach provides a good approximation of the nonlinear behavior of the FPZ provided that the structure is sufficiently large compared to the crack size.

The size effect in geometrically similar structures is generally characterized by the effect of structure size D on the nominal

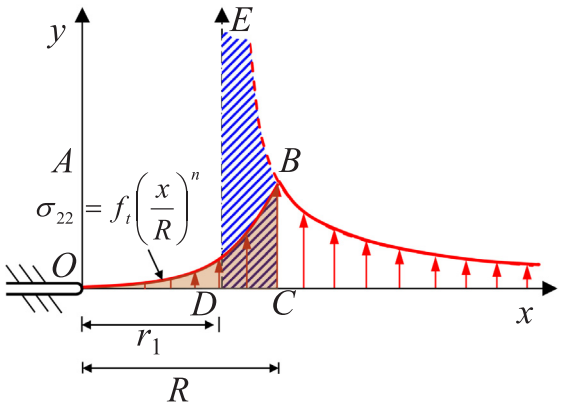

Fig. 1. Equivalent crack for a progressively softening material with cohesive stresses described by a parabolic distribution of degree n.

strength $\sigma_N = c_s P/A$ which is a measure of the load P with a dimension of stress; c_s = conveniently chosen dimensionless constant, used to make σ_N equal to the stress at a certain chosen point (for beam specimens, we choose $c_s = 3L/2D$ where L = beam length); A = characteristic cross section area. For two-dimensional scaling, $A = bD$ where b = structure width, and D = characteristic structure size. Both D and A must be measured at homologous locations. For the case of elastic and elastoplastic behaviors, σ_N is constant, which is considered as the case of no size effect.

Let us consider a crack of effective length $a = a_0 + c_f$, where a_0= initial crack length and $c_f = r_1$= effective FPZ length, proportional to Irwin's characteristic length $l_{ch} = EG_f/f_t^2$ [75] and regarded as a material property [61]. The initial relative crack length $\alpha_0 = a_0/D$ at maximum load is assumed to be a constant, which is usually true for structures of different sizes and in fracture specimens is enforced by cutting similar notches. Following LEFM, the energy release rate can be written as follows [50]:

$$G(\alpha) = \frac{\sigma_N^2 D}{E'} g(\alpha) \tag{1}$$

where $\alpha = a/D$= normalized effective crack length; $E' = E$= Young's modulus for plane stress and $E' = E/(1-\nu^2)$ for plane strain with ν= Poisson's ratio; and $g(\alpha)$= dimensionless energy release function. Note that $g(\alpha)$ accounts for geometry effects and can be calculated by finite element analysis (FEA) or using the fracture mechanics handbooks (see e.g. [76,77]). We may consider that σ_N attains its peak value, referred to as the nominal strength σ_{Nc} of the structure, when the energy release rate at the equivalent crack tip reaches a critical value. Therefore, we have

$$G(\alpha_0 + c_f/D) = \frac{\sigma_{Nc}^2 D}{E'} g(\alpha_0 + c_f/D) = G_f \tag{2}$$

where G_f is the initial mode I fracture energy of the material (i.e., the area under the initial tangent of the softening curve $\sigma(w)$ of cohesive stress σ versus crack opening w [39,61] as shown in Fig. 2) and c_f is the effective FPZ length, both assumed to be material properties. Note that this equation characterizes the peak load if $g'(\alpha) > 0$, which is called the case of positive geometry [50].

By approximating $g(\alpha)$ with its Taylor series expansion at $\alpha = \alpha_0$ and retaining only the first two terms, one obtains:

$$G_f = \frac{\sigma_{Nc}^2 D}{E'}\left(g(\alpha_0) + \frac{c_f}{D} g'(\alpha_0)\right) \tag{3}$$

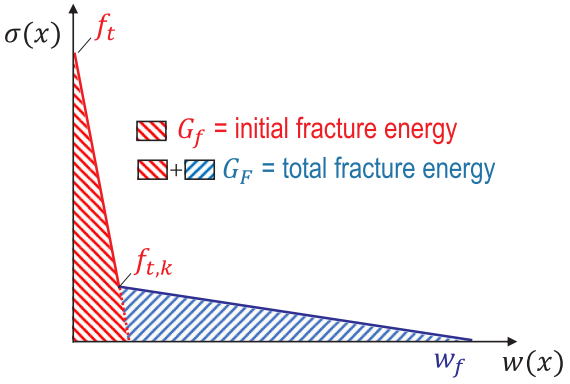

Fig. 2. Bi-linear cohesive law featuring the initial fracture energy, G_f, and the total fracture energy, G_F.

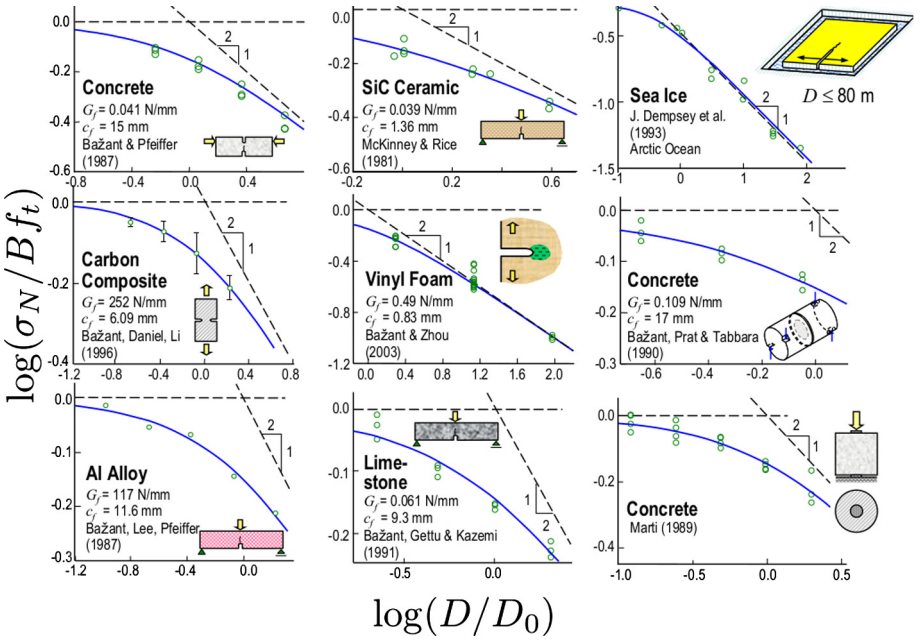

Fig. 3. Optimum fitting of size effect data by using Eq. (5).

which can be rearranged in the following form [50]:

$$\sigma_{Nc} = \sqrt{\frac{E' G_f}{D g(\alpha_0) + c_f g'(\alpha_0)}} \tag{4}$$

where $g'(\alpha_0) = \mathrm{d}g(\alpha_0)/\mathrm{d}\alpha$.

This equation relates the nominal strength of geometrically scaled structures to a representative size, D. It can be rewritten in the following form:

$$\sigma_{Nc} = \frac{B f_t}{\sqrt{1 + D/D_0}} \tag{5}$$

where $B f_t = \sqrt{E' G_f / c_f g'(\alpha_0)}$ and $D_0 = c_f g'(\alpha_0)/g(\alpha_0)$ are constants, depending on both FPZ size and specimen geometry (f_t = tensile strength, introduced to make B dimensionless). Thanks to the functions $g(\alpha)$ and $g'(\alpha)$, Eqs. (4) and (5) explicitly account for geometry effects and can be readily applied to any structure geometry and relative crack length. Contrary to the classical theory of LEFM, Eq. (5) is endowed with a characteristic length scale D_0. This is the key to describe the transition from quasi-ductile to brittle behavior with increasing structure size, as seen in all quasibrittle structures. As can be noted from Fig. (3), which shows the fitting of size effect data of several quasibrittle materials, the agreement between Type 2 SEL and experiments is excellent.

It may be emphasized that Eqs. (4) and (5) are rigorously derived from fracture mechanics by introducing an effective FPZ length and using Taylor series expansion of the dimensionless energy release rate function. No empirical argument has been made. Furthermore, it has been shown that Eqs. (4) and (5) can be derived by leveraging other rigorous mathematical approaches, including the dimensional analysis and asymptotic matching [51] (see the Appendix section in the present manuscript) and cohesive zone modeling [61]. Eq. (5), without Eq. (4), can also be derived from dimensional analysis and the conditions of energy conservation during crack growth, without any recourse to fracture mechanics; see the Appendix.

It is worth noting that Eqs. (4) and (5) depend on only two fracture material parameters: the initial fracture energy G_f and the effective FPZ size c_f. The elastic modulus E' can be characterized from uniaxial tests whereas $g(\alpha)$ and $g'(\alpha)$ can be calculated for any geometry and crack length by finite element analysis. Furthermore, cohesive zone modeling by Cusatis and Schauffert [61] showed that an explicit relation exists between the effective FPZ length c_f and Irwin's characteristic length $l_{ch} = E^* G_f / f_t^2$. They showed that, for a linear cohesive law, $c_f \approx 0.44 l_{ch} = 0.44 E^* G_f / f_t^2$. This illuminating relation indicates that Eqs. (4) and (5) can be used not only to estimate the initial fracture energy but also the strength of the material. More importantly, Cusatis and Schauffert's results prove, unequivocally, that the Type 2 Size Effect Law (SEL), Eqs. (4) and (5), can be derived as the large size asymptote of the cohesive zone model. This is another confirmation of the validity of SEL.

3.2. Size effect for Crack Initiation (Type 1 size effect)

The Type 1 size effect applies to structures for which there is no notch, i.e. $a_0 = 0$. In this case, the size effect is induced by both stress redistribution in the emerging FPZ and the randomness of material strength. The effects of the FPZ can be captured by an

equivalent LEFM approach similar to the one used to derive the Type 2 size effect. Since, for specimens with no notches, the first term of the dimensionless energy release rate function is zero ($g(0) = g_0 = 0$), one can truncate the Taylor series expansion of $g(\alpha)$ only after the quadratic term. Then, substituting into Eq. (2) and rearranging, one gets [78]:

$$\sigma_{Nc} = \sqrt{\frac{E^* G_f}{c_f g'(0) + \frac{1}{2} g''(0) c_f^2 / D}} \tag{6}$$

Eq. (6) may be approximated as

$$\sigma_{Nc} = f_{r\infty}(1 - x)^{-1/2} \tag{7}$$

$$\text{where } f_{r\infty} = \sqrt{\frac{E^* G_f}{g_0' c_f}}, \quad x = \frac{-g_0''}{g_0'} \frac{c_f}{2D} \tag{8}$$

Because only the first two terms of the expansion matter, Eq. (7) can further be equivalently replaced by any binomial expansion that retains the first two terms. Therefore, it is legitimate to replace this equation by

$$\sigma_{Nc} = f_{r\infty}(1 + x)^{1/2} \quad \text{or} \quad \sigma_{Nc} = f_{r\infty}[1 + r(x/2)]^{1/r} \tag{9}$$

where r is an arbitrary positive number determined by optimum fitting of the experimentally measured size effect curve (the modification by Eq. 9 is not only legitimate but also necessary to avoid wrong small-size asymptotics). Upon setting $x/2 = D_b/D$ where

$$D_b = \left\langle \frac{-g_0''}{4 g_0'} \right\rangle c_f \tag{10}$$

one gets the final form of the Type 1 size effect law (Fig. 4a):

$$\sigma_{Nc} = f_{r\infty}\left(1 + \frac{r D_b}{D}\right)^{1/r} \tag{11}$$

where $\langle x \rangle$, defined as $\max(x, 0)$, is used in Eq. (10) because the ratio g_0''/g_0' can sometimes be positive, in which case there can be no size effect, i.e., D_b must vanish.

It should be pointed out that Eq. (11) not only has the correct first and second-order asymptotic properties for $D \to \infty$, like Eq. (7), but also has a realistic form for small D, such that $\lim_{D\to 0}\sigma_N$ be neither 0 nor imaginary. The fact that the limit $\sigma_N \to \infty$ is shared by the famous, widely used, Petch-Hall formula for the effect of crystal size in polycrystalline materials [79] is incidental. In fact, based on the cohesive crack model, the limit for σ_{Nc} is finite, but this does not matter in practice because D cannot be less than about three maximum aggregate sizes, as the material could no longer be treated as a continuum.

The foregoing derivation of Type 1 size effect is anchored solely by the energetic analysis of the fracture process. It predicts a vanishing size effect at the large size limit. For this reason Eq. (11) is often called the *energetic* since it accounts for the energetic size effect induced by the stress redistribution in the FPZ but not for the one produced by the randomness of material strength. However,

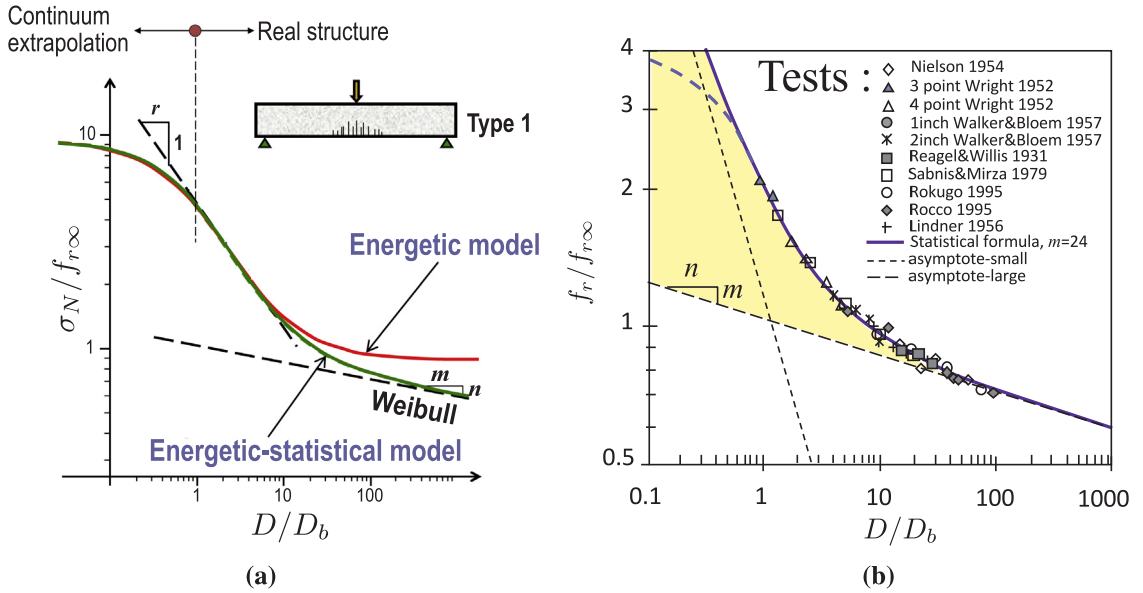

Fig. 4. Type 1 size effect: (a) schematic of energetic and energetic-statistical Type 1 size effect curves, and (b) comparison with experimental data.

for very large size structures, the size effect of this type tends to be statistical, which is due to fact that the Type 1 failure can initiate at many different locations within the material, whose strength is a random field. Thus, in a larger structure, the minimum of the random material strength tends to be smaller. This randomness inevitably leads to the classical Weibull size effect (Fig. 4a) [12]. To amalgamate the random and energetic triggers of failure, it is thus necessary to combine Eq. (11) and the classical Weibull size effect to form an energetic-statistical size effect equation for Type 1 failures [74,78]:

$$\sigma_{Nc} = f_{r\infty}\left[\left(\frac{D_a}{D}\right)^{rm/m} + \frac{rD_b}{D}\right]^{1/r} \tag{12}$$

where D_a= constant, m= Weibull modulus, and n= number of spatial dimensions in which the failure mode and the structure are scaled. Since Eq. (12) accounts for both the energetic and statistical sources of size effect, it is often referred to as the *energetic-statistical size effect law*

Fig. 4b shows the comparison between Eq. (12) and the available experimental data on concrete beams from ten different labs [53,54]. It is worth noting that Eq. (12) was obtained by a rigorous combination (asymptotic matching) of fracture mechanics and statistics [53,54]. An alternative derivation resting on a nano-mechanics based failure probability theory is given in [12,63].

Note that the number of free material parameters in the *energetic law*, Eq. (11), and *energetic-statistical law*, (12), is quite limited. In fact, the dimensionless energy release functions $g'(0)$ and $g''(0)$ can be calculated by finite element analysis, and so only c_f needs to be determined to characterize D_b. Accordingly, for cases in which the statistical effects are not significant, i.e., for the *energetic model* Eq. (11), the parameters are only three: c_f (which can be correlated to the material strength and initial fracture energy by cohesive zone modeling), r, and $f_{r\infty}$. For cases in which the effects of material strength randomness are significant, the *energetic-statistical model* Eq. (12) can be used. In such a case the parameters are: c_f, r, D_a, m and $f_{r\infty}$. Note that D_a is an additional parameter that describes the transition from energetic to statistical size effect whereas m is the Weibull modulus, which controls the statistical size effect on the mean behavior.

4. Description of boundary effect model

According to BEM, the size effect on structural strength is caused solely by the interaction between the FPZ and the boundary of the structure [31,35–37]. The BEM was derived in an empirical way, starting from the analysis of an edge crack in a semi-infinite plate at incipient failure. In that case:

$$K_{Ic} = Y\sqrt{\pi a_0}\sigma_{Nc} \tag{13}$$

where σ_{Nc}= nominal critical stress in the gross cross section, $Y = 1.12$ and K_{Ic}= material fracture toughness. Setting $\sigma_{Nc} = f_t$ and rearraning Eq. (13), Hu et al. defined the following transitional crack length:

$$a_\infty^* = \frac{1}{1.12^2\pi}\left(\frac{K_{Ic}}{f_t}\right)^2 \approx \frac{1}{4}\left(\frac{K_{Ic}}{f_t}\right)^2 \tag{14}$$

which is, of course, proportional to the well-known Irwin's characteristic length [75], because $a_\infty^* \approx l_{ch}/4$ for plane stress and $a_\infty^* \approx l_{ch}/[4(1-\nu^2)]$ for plane strain are constants. For large-size structures, Hu et al. proposed that the failure condition should scale as LEFM. Accordingly,

$$1.12\sqrt{\pi a_0}\sigma_{Nc} = 1.12\sqrt{\pi a_\infty^*}f_t = K_{1c} \tag{15}$$

which leads to the following scaling law:

$$\sigma_{Nc} = \frac{f_t}{\sqrt{a_0/a_\infty^*}} \tag{16}$$

Then, by claiming that, for small sizes, $a_0 \to 0$, the nominal strength should approach f_t, Hu et al. postulated the following equation without any physical justification:

$$\sigma_{Nc} = \frac{f_t}{\sqrt{1 + a_0/a_\infty^*}} \tag{17}$$

which, unsurprisingly and conveniently, takes a similar form as the Type 2 SEL.

Eq. (17) was derived by Hu et al. for very large plates weakened by an edge crack. For a finite size plate, they defined a different nominal stress as the maximum stress in the net cross section, σ_n, which they suppose to account for the finiteness of the cross section. Without any justification, they assumed the stress distribution to be linear (Fig. 5a), and calculate σ_n by imposing equilibrium between the gross and net sections. Thus they obtain:

$$\sigma_n = \frac{\sigma_{Nc}}{A(\alpha_0)} \tag{18}$$

where $\alpha_0 = a_0/D$, and $A(\alpha)$ is a dimensionless function dependent on the crack length and the structure geometry.

The foregoing procedure leads to $1.12\sqrt{\pi a_\infty^*}f_t = Y(\alpha_0)\sqrt{\pi a_0}\sigma_{Nc}$, and so

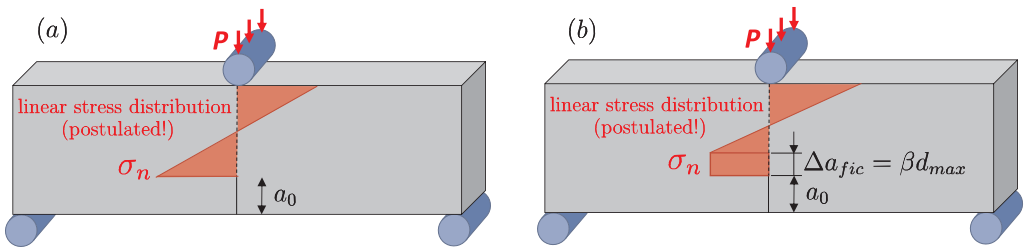

Fig. 5. Stress distribution in the ligament assumed without justification in the (a) old version of BEM [34–36] and (b) latest version of BEM [37].

$$\sigma_n A(\alpha_0) = \frac{f_t}{\sqrt{[Y(\alpha_0)/1.12]^2 a_0/a_\infty^*}} \tag{19}$$

Finally,

$$\sigma_n = \frac{f_t}{\sqrt{a_e/a_\infty^*}} \tag{20}$$

where $a_e = [A(\alpha_0)Y(\alpha_0)/1.12]^2 a_0$= equivalent crack length accounting for geometry effects.

Hu et al. then again conveniently assumed the following scaling relation to link the small- and large-size asymptotes:

$$\sigma_n = \frac{f_t}{\sqrt{1 + a_e/a_\infty^*}} \tag{21}$$

It is worthwhile to discuss the role of the nominal stress definition in the BEM (Eq. (21)). It is noted that the derivation of the Type 1 and Type 2 SEL (Eqs. (11) and (5)) hinges on the energy release function, which gets automatically adjusted for different definitions of σ_{Nc}. Therefore, the final size effect equations are not affected by the definition of nominal strength. One may use any convenient choice such as the average stress in the gross cross section [76,77,80–85]. However, this is not the case for the BEM. The BEM was derived based on a particular definition of the nominal stress, which assumes a linear stress distribution along the ligament. As will be shown later, such a stress profile is just a fiction and differs grossly from the real stress distribution. This unrealistic assumption directly enters the BEM equation, without any physical argument (Eq. (19)).

Attempting to correct various discrepancies, Hu et al. [37] introduced in the latest version of the BEM an additional artificial concept, referred to as the "fictitious crack" (the same term as used by Hillerborg for a cohesive crack in his version of the cohesive crack model for concrete). Their intent is to account, with the fictitious crack length, Δa_{fic}, for the effects of aggregate size; $\Delta a_{fic} = \beta d_m$, where d_m, representing the maximum aggregate size, becomes an additional material parameter to be identified by fitting the experimental data. The stresses were assumed to be uniform along the initial fictitious crack and then to follow a linear distribution in the remaining part of the ligament. Fig. 5b shows a schematic adapted from [37], describing the stresses in a typical three-point bending (3 PB) specimen. The relation between σ_n and the applied load P_{max} is then found by imposing equilibrium. Based on Fig. 5, the nominal stress for a 3 PB specimen can be calculated as follows:

$$\begin{aligned}\sigma_n &= P_{max}\frac{3SL_g^2/B_T}{(L_g+\beta d_m)^3(L_g-\beta d_m)+(L_g-\beta d_m)^4+6L_g d_m(L_g^2-L_g\beta d_m+\beta^2 d_m^2)}\\ &= P_{max}\frac{3/d_m\eta l^3/B_T}{(l+\beta)^3(l-\beta)+(l-\beta)^4+6\beta l(l^2-\beta l+\beta^2)}\\ &= P_{max}\frac{3\eta/B_T}{2d_m(l+2\beta)}\end{aligned} \tag{22}$$

where S= beam span, $l = L_g/d_m \geqslant 1$, $L_g = D - a_0$= ligament length, B_T= specimen thickness and $\eta = S/L_g$. Following Hu et al. [37], the peak load is then calculated combining Eqs. (21) and (22):

$$\sigma_n(P_{max}, \beta d_m, l, \eta) = \frac{f_t}{\sqrt{1+\frac{a_e}{a_\infty^*}}} \tag{23}$$

The foregoing equation describes the size effect on the nominal stress resulting from postulating the stress field in the ligament, σ_n.

In the present contribution, to make a proper comparison with the experimental data and SEL, Eq. (23) is rewritten from Eq. (22) in terms of the nominal stress defined in a usual way as $\sigma_{Nc} = 3SP_{max}/2D^2B_T$:

$$\begin{aligned}\sigma_{Nc} &= \frac{3P_{max}S}{2D^2B_T} \\ &= \frac{3P_{max}\eta(1-\alpha_0)}{2DB_T} \\ &= \frac{f_t(1-\alpha_0)}{\sqrt{1+a_e/a_\infty^*}}(l+2\beta)\frac{d_m}{D} \\ &= \frac{f_t A(\alpha_0)}{\sqrt{1+D(\alpha_e/a_\infty^*)}}\left(1+2\beta\frac{d_m}{D\sqrt{A(\alpha_0)}}\right)\end{aligned} \tag{24}$$

where $\alpha_e = a_e/D = a_e = [A(\alpha_0)Y(\alpha_0)/1.12]^2\alpha_0$ and $A(\alpha_0) = (1-\alpha_0)^2$ for 3 PB specimens.

The foregoing BEM model depends on 3 parameters in total: the tensile strength f_t, the mode I fracture toughness K_{Ic} and the parameter β that relates the size of the fictitious crack to the maximum aggregate size. According to Hu et al. [37], parameter β may change with the structure size. However, the dependence of β on the structure size is not provided. Hu et al. propose using the median among the values of β that provide the best fit of the experimental data for different specimen sizes and different initial crack lengths. This kind of proposition precludes, of course, any predictive capability of the model. The value of β may lead to a satisfactory fit only within the range of experimental data.

Finally, it should be stressed again that Eq. (24) has been obtained in an empirical way. Why does the effect of the equivalent crack take the form $1/\sqrt{1+a_e/a_\infty^*}$ and not $1/\sqrt{1/2+a_e/a_\infty^*}$, or $A/\sqrt{a_e/a_\infty^*}$? Since Hu et al. obtained this expression empirically there is no answer to this question. In particular, the fact that Hu et al. did not verify the asymptotic behavior of this expression is a serious deficiency, as comparisons with the cohesive zone modeling and the bulk of experimental data will reveal in the sections that follow.

5. Deficiencies of BEM and comparisons to SEL

The limitations and inconsistencies of the previous versions of BEM were identified and comprehensively discussed in previous two papers [39,40]. The new version of BEM [37] not only persists in most of these deficiencies but also introduces new fundamentally flawed concepts. This section will focus on the deficiencies of the new version whereas those of the older versions will be reviewed only briefly.

5.1. Application of BEM to Type 2 failures

The latest version of the Boundary Effect Model (BEM) [37] introduces the idea of using the maximum aggregate size d_m to define the stress profile (Fig. 5) and thus allows a more accurate prediction of the tensile strength. This idea, however, is fundamentally flawed. Based on the stress profile depicted in Fig. 5, BEM considers the nominal strength σ_{Nc} to be related to the strength σ_n as

$$\sigma_{Nc} = \sigma_n(1+\beta d_a/D) \tag{25}$$

This scaling relation, which is the consequence of introducing a fixed length scale d_m into the stress profile, is similar to the boundary layer model for the size effect on the modulus of rupture [86]. By further imposing a size effect on σ_n, Eq. (21), the latest version of the BEM, Eq. (24), yields the scaling relation for the nominal strength, σ_{Nc}:

$$\sigma_{Nc} \propto (1+\zeta D/a_\infty^*)^{-1/2}(1+\beta d_m/D) \tag{26}$$

This scaling equation predicts that: (1) $\sigma_{Nc} \propto D^{-1}$ at the small-size limit ($D \to 0$), and (2) $\sigma_{Nc} \propto D^{-1/2}$ at the large size limit ($D \to \infty$). But the small-size asymptotic behavior is blatantly unrealistic. It violates the second-order asymptotic properties of the cohesive crack model. As will be shown in Section 5.1, in contrast to SEL, the deviation of BEM from cohesive fracture mechanics occurs well before the structure size D gets close to the aggregate size.

This deficiency can be demonstrated by comparing SEL and BEM to the size effect curves obtained by means of the cohesive zone model. Assuming, for simplicity, a linear cohesive law, and following Cusatis and Schauffert [61], it is convenient to rewrite Eq. (24) in the form $\xi = F(X)$ with $\xi = 1/g_0'(f_t/\sigma_N)^2$ and $X = g_0 D/g_0' l_{ch}$. Assuming further a plane strain condition, one can find the following relationship between the dimensionless energy release rate $g(\alpha_0)$ and the geometry function $Y(\alpha_0)$:

$$g(\alpha_0) = \pi\alpha_0(1-\nu^2)Y(\alpha_0)^2 \tag{27}$$

Then, starting from Eq. (24) and rearranging, one obtains:

$$\xi = \frac{1}{g_0'}\left(\frac{f_t}{\sigma_N}\right)^2 = \left(\frac{1}{A(\alpha_0)^2 g_0'} + X\right)\left(1+2\beta\frac{g_0 d_m/l_{ch}}{X g_0'\sqrt{A(\alpha_0)}}\right)^{-2} \tag{28}$$

On the other hand, considering that, according to [61], $c_f \approx 0.44E^*G_f/f_t^2$, Type 2 SEL, Eq. (4), can be written as follows:

$$\xi = 0.44 + X \tag{29}$$

While both BEM and SEL predict a linear relation between ξ and X for large sizes, the intercept in BEM depends significantly on the particular structural geometry under consideration, the relative crack length α_0 and the maximum aggregate size d_m. This dependence disagrees with cohesive fracture mechanics. Cusatis et al. [61] showed that, for a linear cohesive law, $F(X)$ tends asymptotically to SEL with an intercept equal to 0.44 regardless of the structure or specimen geometry, and of the relative crack length.

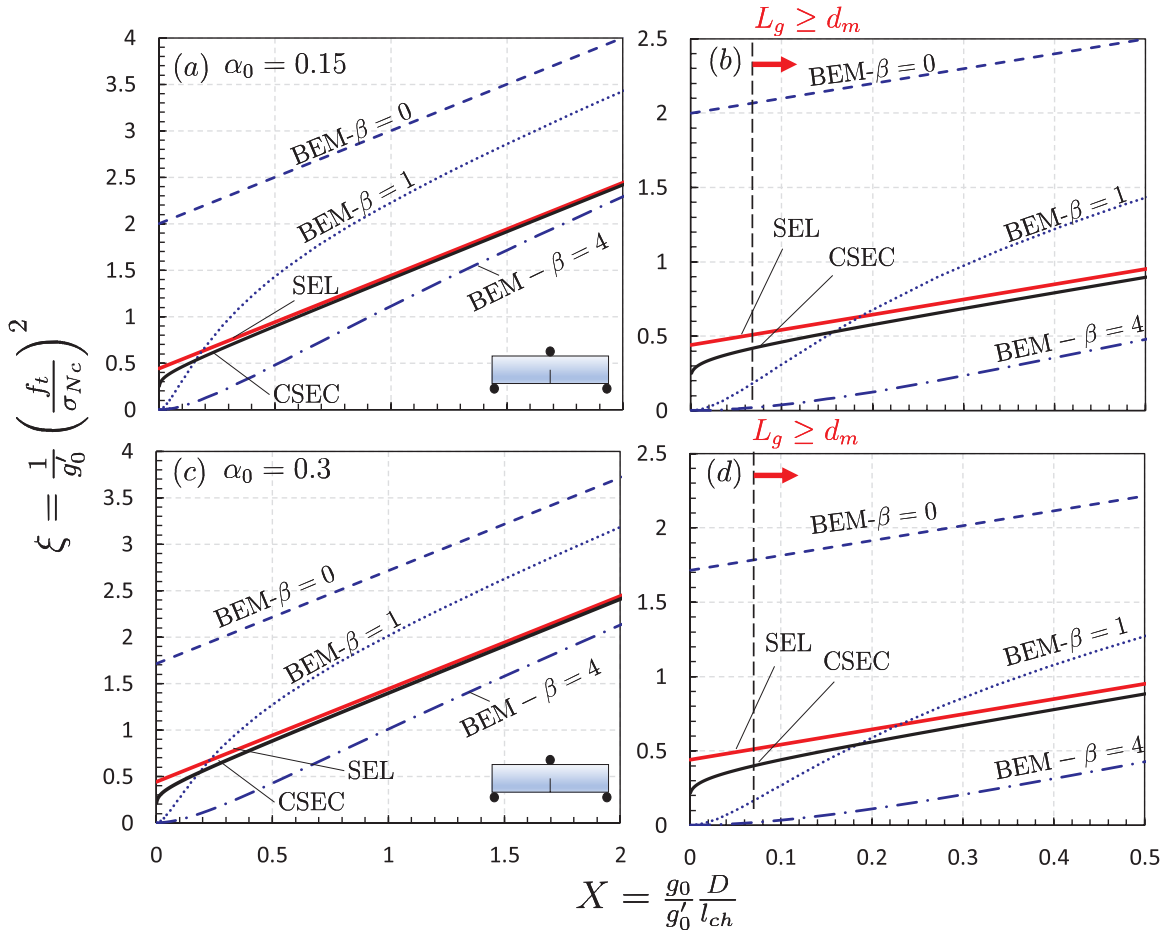

Fig. 6. Comparison between Size Effect Law (SEL), Boundary Effect Model (BEM) and Cohesive Size Effect Curve (CSEC) for geometrically-scaled three-point bending specimens and different initial notch lengths: (a) case $\alpha_0 = 0.15$ and (b) related magnification for lower X values; (c) case $\alpha_0 = 0.3$ and (b) related magnification for lower X values. The following material properties are used: $E = 40$ GPa, $\nu = 0.18$ (typical elastic properties of concrete), $f_t = 5.56$ MPa and $K_{Ic} = 1.49$ MPa m$^{1/2}$ and $d_m = 10$ mm (data taken from [37]).

To exemplify the problem, let us compare the size effect curves obtained by cohesive fracture mechanics for a linear cohesive law to the ones predicted by SEL and BEM, considering geometrically-scaled three-point bending (3 PB) specimens. In that case, for $S/D = 4$, according to Anderson [85],

$$A(\alpha) = (1-\alpha)^2$$
$$Y(\alpha) = \frac{1.99 - \alpha(1-\alpha)(2.15 - 3.93\alpha + 2.7\alpha^2)}{\sqrt{\pi}(1+2\alpha)(1-\alpha)^{3/2}}$$

The foregoing expressions can be used to calculate the size effect curve predicted by BEM, Eq. (28). For the cohesive crack model, the size effect curve has been calculated from the following expression proposed by Cusatis [61]:

$$\xi = X + \frac{1 + 11\sqrt{X}}{9(1-\alpha)^4 g_0' + 25\sqrt{X}} \tag{30}$$

Fig. 6a–d show a comparison between SEL, BEM and the Cohesive Size Effect Curves (CSEC) for two dimensionless crack lengths, namely $\alpha_0 = 0.15$ and 0.3. For the calculations, the following material properties are used: $E = 40$ GPa and $\nu = 0.18$ (typical elastic properties of concrete), $f_t = 5.56$ MPa, $K_{Ic} = 1.49$ MPa m$^{1/2}$ and $d_m = 10$ mm (taken from [37]). It is interesting that while the only parameters required for SEL and CSEC are tensile strength f_t and fracture energy G_f, BEM requires an additional model parameter β related to the maximum aggregate size (instead of just the basic two influencing parameters, f_t and G_f). Yet, notwithstanding the presence of a third fitting parameter, both the small and large-scale asymptotes predicted by BEM are nowhere close to cohesive fracture mechanics.

For $\beta = 0$, corresponding to the old version of BEM [34–36], the size effect predicted by BEM is described by a straight line of unit slope, similar to Type 2 SEL. However, there is a substantial difference: while the CSEC curve always closely agrees with the SEL for small sizes and tends asymptotically to the SEL for sufficiently large sizes, the same is not true for the BEM, which is generally

characterized by a higher intercept, depending on the initial notch length and the specimen geometry through the function $A(\alpha_0)$.

The disagreement, especially in terms of the tangent of the size effect curves, gets worse for values of β other than zero, as proposed in the latest formulation of the BEM [37]. In this case, the small-scale behavior totally differs from CSEC, and there is no possible β-value that could mitigate it. This is not surprising because the BEM introduced an artificial size effect term $(1 + \beta d_a/D)$ (Eq. (25)), which is based on an unrealistic stress distribution. The validity of such a term could easily be checked by asymptotic analysis, which Hu et al. skipped. On the other hand, the SEL shows an excellent agreement, which reflects the physical soundness of the model.

Finally, it is important to note that, aside from conflicting with cohesive fracture mechanics, the asymptotic behavior of BEM disagrees with the bulk of experimental data on quasibrittle materials, as shown next.

5.2. Application of BEM to Type 1 failures

In [37], Hu et al. claimed that the BEM can be applied to Type 1 failures. In the old version of BEM [34–36], Hu et al. imposed for this purpose an initial crack length, a_{eff}, that is proportional to the specimen size, claiming to capture the Weibull size effect. But this claim is groundless. The Weibull size effect applies to quasibrittle structures only if they are very large (i.e., much larger than the inhomogeneity size) and only if they fail at macrocrack initiation. The key statistical characteristic of the Weibull size effect is the Weibull modulus. But the BEM involves no statistical characteristics. Therefore, it cannot capture the Weibull size effect.

The proportionality between the flaw size and specimen size, assumed in [34–36], was also incorrect. Freudenthal showed that the Weibull size effect can be correlated to flaw statistics, for which he assumed the Fréchet distribution of the largest flaw sizes. It is, of course, reasonable to state that for a larger specimen the maximum flaw size will be larger, more critical. However, based on the extreme value statistics (Fréchet distribution), the mean value of the largest flaw size increases only mildly with the specimen size. Assuming the flaw size to be proportional to the specimen size, the BEM would predict the large-size asymptotic scaling of $D^{-1/2}$. Such scaling would, of course, be incorrect, and is never seen in Type 1 size effect tests. The size effect data on three-point and four-point bend tests on concrete materials have consistently shown that the large-size asymptote of the two-dimensional size effect is $D^{-1/12}$ [12,53,54,74,78] which is based on the known Weibull modulus for concrete, $m \approx 24$ (see e.g. Fig. 4).

As mentioned earlier, in the newest version of BEM [37], Hu et al. tried to circumvent the problem by introducing an additional fictitious crack proportional to the maximum aggregate size, $\Delta a_{fic} = \beta d_m$ (see Fig. 5b). The additional fictitious crack is supposed to represent the initial micro-damage that is present even without a stress-free crack or notch, and the stresses along this crack are assumed to be uniform (which is certainly far from reality).

In contrast to the old BEM, the fictitious crack in the new BEM does not influence the definition of the equivalent crack a_e, which is set to 0 in the case of failure at crack initiation. Rather, it influences the definition of the nominal strength σ_n as described in Eq. (22). Setting $\alpha_0 = 0$ and $a_e = 0$ in Eq. (24), which describes the size effect on the nominal strength in the gross section according to BEM, one gets:

$$\sigma_{Nc} = f_t\,(1 + 2\beta d_m/D) \tag{31}$$

It is interesting that this new expression, which was described by Hu et al. as a substantial improvement, resembles the early version of size effect equation on the modulus of rupture [86] (special case of Eq. (12) with $r = 1$). However, it has been shown that the optimum fitting of test data often requires some different values of r. Meanwhile, Eq. (31) predicted an incorrect large-size asymptotic behavior, i.e. $\sigma_{Nc} \to f_t = \text{const.}$. This again contradicts all experimental evidence, as can be noted from, e.g., Fig. 7a and b

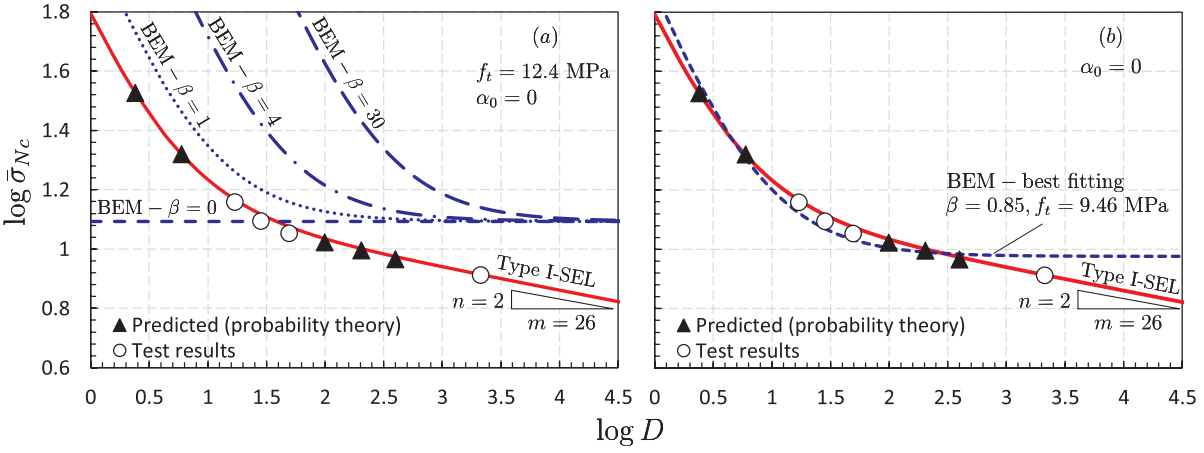

Fig. 7. Fitting of experimental data on geometrically-scaled un-notched specimens made of asphalt concrete by Type 1 Size Effect Law (SEL) and Boundary Effect Model (BEM). Data taken from [64]. The strength is calculated averaging 12 test results for size 1, 28 for size 2, 30 for size 3 and 7 for size 4 [(a) shows the effect of parameter β on BEM]. The strength is fixed at 12.4 MPa, which is the average of 28 tests on size 2 specimens; (b) Best fitting with BEM and Type 1 SEL. A Weibull modulus $m = 26$, as obtained from independent histogram testing, was adopted for Type 1 - SEL.

reporting the test data taken from [64] on geometrically-scaled, notch-free three-point-bending (3 PB) specimens and uniaxial tension specimens made of asphalt mixtures. In these experiments, the size of the uniaxial tension specimen was chosen to be much larger than the aggregate size. Therefore, one may use the classical Weibull theory to determine the mean strength of the tensile specimen. Meanwhile, one can also calculate the mean strength of a 3 PB specimen by the Weibull theory. The equivalent size of the 3 PB specimen that has the same mean strength as the tensile specimen can then be calculated [50,64]. Consequently, the size range in these tests is sufficiently large to show a clear statistical size effect. For the two intermediate sizes of 3 PB beams, histogram testing was performed so that the Weibull modulus of the material can be determined ($m = 26$). As expected, this modulus is reflected in the slope of the large-size asymptote of the average strength as can be noted in Fig. 7a and b.

The experimental data are complemented by the optimum fitting of the finite weakest-link model [12,60,62–64] which can inherently capture the transition from energetic to statistical size effect. As can be noted (Fig. 7a and b), the Type 1 SEL provides an excellent fitting of the data, particularly at the small- and large-size asymptotes. Satisfying the correct asymptotic behaviors is an essential requirement of any physical model. It is important to note that the Type 1 SEL satisfies this requirement, by exploiting parameters such as the Weibull modulus, m, which can be verified independently by other tests, e.g., by strength histogram testing.

Owing to the empiricism of its formulation, the same cannot be said for BEM, which neglects the statistical size effect for large sizes. This is clear in Fig. 7a, which shows the influence of parameter β on the BEM size effect. The strength for these analyzes was set equal to 12.4 MPa, which is the average of 28 tests on size 2 specimens. This is the intermediate size of all the specimens investigated. Any other strength value could have been used to investigate the effects of β without changing the conclusions. For $\beta = 0$, no size effect is predicted, which contradicts experimental data. For increasing values of β, the small-scale asymptote proportional to D^{-1} extends further and further.

For some β-values, the BEM is able to fit some of the small-size data well, but not for large sizes. This is evident in Fig. 7b, which presents the best fit possible of BEM obtained by means of the Levemberg-Marquardt algorithm [87,88]. The underlying reason is that the BEM ignores the statistical size effect, which governs the large-size asymptote. This is a serious issue because the BEM will grossly overestimate the mean strength of large-size structures, which would lead to an unsafe design.

In view of these observations, one might wonder: How, in the latest Hu et al.-s paper [37], could the BEM (Eq. (31)) give an acceptable fit of the experimental data on Type 1 size effect? Obviously, because the size range of the test data fitted was rather limited and the asymptotic behavior, dominated by the statistical effects, was ignored.

5.3. Limited practical applicability

As discussed in the foregoing sections, the application of BEM to finite-size structures relies on an assumed stress distribution along the ligament. In fact, the σ_n used in the BEM represents the maximum stress at the crack tip assuming a linear distribution of stresses in the net section (see Fig. 5a and b). In contrast, the nominal strength $\sigma_N = c_s P/A$ is a generic measure of the load P with a dimension of stress. Here c_s = conveniently chosen dimensionless constant, used to make σ_N equal to the stress at a certain chosen point (for beam specimens, we choose $c_s = 3L/2D$ where L = beam length).

In standard Mode I fracture specimens, and only if the specimen geometry, including a/D, does not change, σ_n and σ_N are mutually proportional and thus the size effects are the same.

However, for geometries other than simple Mode I fracture specimens, the definition of the stress profile is usually ambiguous. In fact, the fracture process may occur under mixed mode conditions, or the direction angle ϕ in which the ligament will crack may be *a priori* unclear (Fig. 8a–c). Further, the ratio of bending moment M to normal force N in the ligament may often be statically indeterminate (Fig. 8d,f) and, in some cases, the stress profile cannot even be defined (Fig. 8e–h). For all the foregoing situations, the function $A(\alpha_0)$ cannot be calculated. Hence, BEM cannot be applied.

By contrast, the size effect law does not rely on knowing the direction of crack propagation. Rather, it relies on the energy release rate at the crack tip. The dimensionless energy release rate function $g(\alpha_0)$ used in SEL can be unambiguously and easily calculated for all these cases. For example, despite the complex shape of the dominant cracks, the SEL is applicable to the shear failure of reinforced concrete beams and to punching shear failure of slabs (and, for both, is included in the 2019 version of ACI Building Code, ACI Standard 318).

5.4. Groundless assumption of stress profile in the ligament

It has been pointed out that the BEM strongly relies on the definition of the stress profile in the ligament, which directly affects the size effect equation. Therefore, it is important to examine the correctness of the assumed stress profile. The latest version of the BEM [37] assumes a uniform stress profile within a portion of the ligament whose length is proportional to the maximum aggregate size, and a linear stress profile through the rest of the ligament. This assumption is in conflict with the cohesive zone model simulations for any structure size, as can be noted from Fig. 9a–c that compare the stress distributions at peak load postulated by BEM to those predicted by a cohesive zone model featuring a simple linear softening cohesive law.

The simulations were done for 3 PB specimens with span-depth ratio $S/D = 4$, $E = 40$ GPa, $\nu = 0.18$ (typical elastic properties of concrete), $f_t = 5.56$ MPa, and $K_{Ic} = 1.49$ MPa m$^{1/2}$ (taken from [37]). The cohesive law was implemented in a FE model in ABAQUS/Explicit [89]. The models combined 4-node bi-linear plain-strain quadrilateral elements (CPE4R) with a linear elastic isotropic behavior and 4-node two-dimensional cohesive elements (COH2D4) with a linear traction-separation law to model the crack. For BEM, the maximum aggregate size $d_m = 10$ mm was used. Three cases were considered: (a) ligament length $L_g \approx 6l_{ch}$, corresponding to a typical medium size specimen, (b) $L_g \to l_{ch}$, and (c) $L_g \to d_m$.

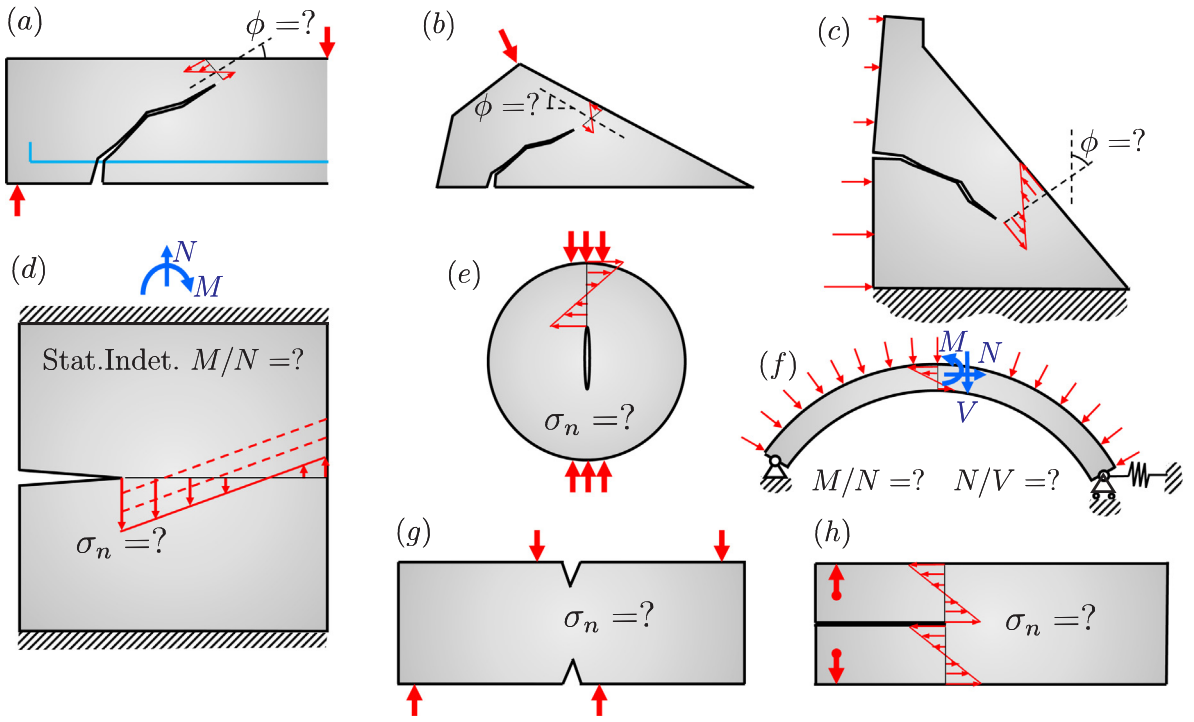

Fig. 8. Examples of specimens and structures for which SEL can be used and BEM cannot.

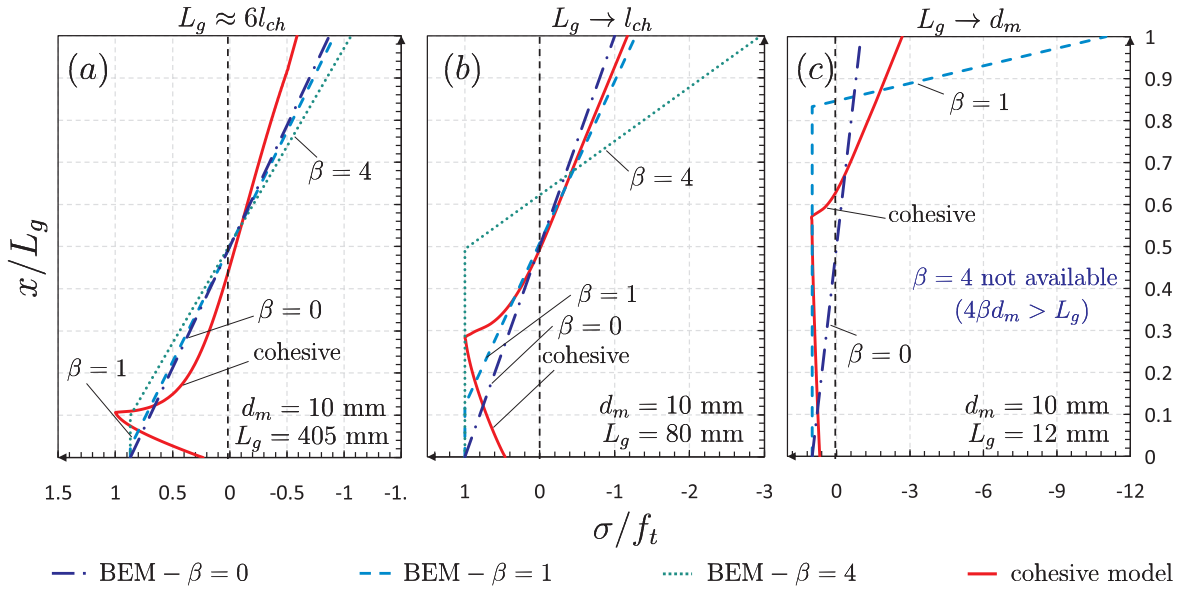

Fig. 9. Stress distribution along the ligament of a 3 PB specimen contrasting BEM versus a cohesive zone model featuring a linear cohesive law: (a) $L_g \approx 6l_{ch}$, (b) $L_g \to l_{ch}$ and (c) $L_g \to d_m$. For all the simulations $S/D = 4$, $E = 40$ GPa, $\nu = 0.18$ (typical elastic properties of concrete), $f_t = 5.56$ MPa and $K_{Ic} = 1.49$ MPa m$^{1/2}$ (taken from [37]).

When the specimen size is finite but relatively large compared to Irwin's characteristic length, Fig. 9a, the FPZ may not be fully developed, as shown by the normalized plot of the predicted cohesive stresses. For this case, the cohesive stresses take a nonzero value at the crack tip and increase monotonically up to the point of tensile strength limit, which advances through the ligament. Beyond that point, the stress decreases monotonically and turns to compression in the upper part of the ligament. The stress distribution postulated in BEM is nowhere close this picture, regardless of the β value. This is particularly evident if one considers the cases in Fig. 9b and c. When the ligament is close to l_{ch}, as shown in Fig. 9b, the crack openings at peak load are significantly smaller compared to the previous case.

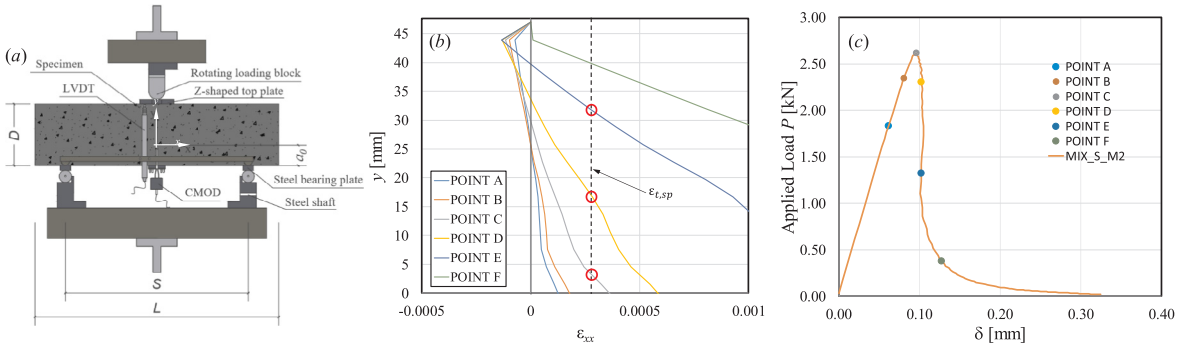

Fig. 10. Experimental characterization of the strain in the ligament of three-point-bending specimens made of Alkali Activated Mortar (AAM): (a) test setup; (b) strain profile at different loading conditions; (c) load-diplacement curve and corresponding loading conditions.

Hence, the stress at the crack tip is nonzero and closer to the material strength. Moving away from the tip, the stress increases up to strength limit and then decreases abruptly in the remainder of the ligament. Since the relative distance from the tip to reach the tensile strength point is larger than it is in the previous case, the equilibrium requires a higher negative slope. These aspects, of course, cannot be captured by BEM.

For the case of $\beta = 0$ (which corresponds to the old version of BEM [34–36]), the slope of the linear stress distribution must be constant. For $\beta = 1$, the approximation is slightly improved in the second part of the ligament but the approximation of the stresses in the FPZ remains still very coarse. For $\beta = 4$, the initial overestimation of the stresses caused by the assumption of uniform distribution leads to a significant overestimation of the negative slope of the ligament portion described by a linear distribution. Similar conclusions can be drawn for the case $L_g \to d_m$, Fig. 9c, for which BEM predicts a uniform stress distribution equal to f_t followed by a linear stress distribution with an infinite negative slope.

The foregoing observations are also supported by recent experimental analyzes obtained by Digital Image Correlation (DIC) which completely disprove the stress distribution assumed in BEM [52]. Dr. Carloni, in collaboration with Dr. Maria Chiara Bignozzi from University of Bologna, have recently conducted a pilot study on Alkali Activated Mortars (AAM). The fracture properties of the mortars have been determined from three-point bend tests of notched beams following a draft of the report prepared by ACI 446 Committee (Fig. 10a). The dimensions of the notched beams were 70 mm (width B) −70 mm (depth D) 300 mm (length L). The net span S was equal to $3D$. The notch a_0 was $D/3$. Digital image correlation was used to determine the strain profile along the ligament.

An example of the strain profile is reported in Fig. 10b, which refers to an AAM with coal Fly Ash (FA) as precursor for the synthesis. FA was characterized by a low content of calcium and iron oxides, while nearly 80 wt% was made of silicon and aluminum oxides. As alkaline activators, 8 M sodium hydroxide and sodium silicate solutions were used. Fine silica sand with maximum aggregate size $d_a = 2$ mm was used. The strain profile along the ligament was obtained by averaging ε_{xx} over a 5 mm strip centered with respect to the notch. The strain profiles of Fig. 10b correspond to different points of the load-load point displacement ($P - \delta$) curve reported in Fig. 10c. A vertical dashed line indicates the tensile strain $\varepsilon_{t,sp}$ corresponding to the splitting tensile strength measured at the age of testing. The intersection between the strain profile and the dashed line corresponding to $\varepsilon_{t,sp}$ is indicated with a marker for points C, D and E of Fig. 10c. It can be observed that the neutral axis moves upward as the Fracture Process Zone (FPZ) develops. At point C, which corresponds to the peak load, the distance from the notch tip to the marker that indicates the beginning of the FPZ can be estimated to be $2d_a$.

5.5. Lack of mathematical basis for asymptotic matching

Since the procedure to set up BEM was intuitive and empirical, it is no surprise that no use was made of any systematic matching of the two-sided second-order asymptotic properties characterizing the way the asymptotes are approached. In the spirit of this intuitive procedure, there is no reason for not using, e.g., $\sigma_n = f_t/\sqrt{1/2 + a_e/a_\infty^*}$, or any other variant with the same asymptotes instead of Eq. (21). Probably the tacit reason for choosing Eq. (21) was to arrive at an expression similar, though not identical, to Type 2 SEL, because the SEL has become, for quasibrittle materials, a generally accepted theoretical result with solid experimental support.

It should be emphasized, though, that the SEL, unlike BEM, was derived by matching the second-order asymptotic properties of the cohesive crack model [39,61] or the equivalent LEFM [1]. This difference is conspicuous in the comparisons of SEL, BEM and the cohesive zone model presented in the previous sections.

5.6. Comparison with experimental data and comments on Hu's optimum data fitting

Fig. 11a and b compare the analysis of Hoover et al.'s tests on geometrically-scaled, notched concrete beams [41,42] by SEL and by the latest version of the BEM, for two different initial notch lengths: $\alpha_0 = 0.15$ and $\alpha_0 = 0.3$. To asses the predictive capability of the two models, both SEL and BEM were calibrated by best fitting of the experimental data for the notch length $\alpha_0 = 0.15$ (Fig. 11a). The fitting was based on all the experimental data, in order to consider the scatter. Then, the calibrated set of parameters was used to

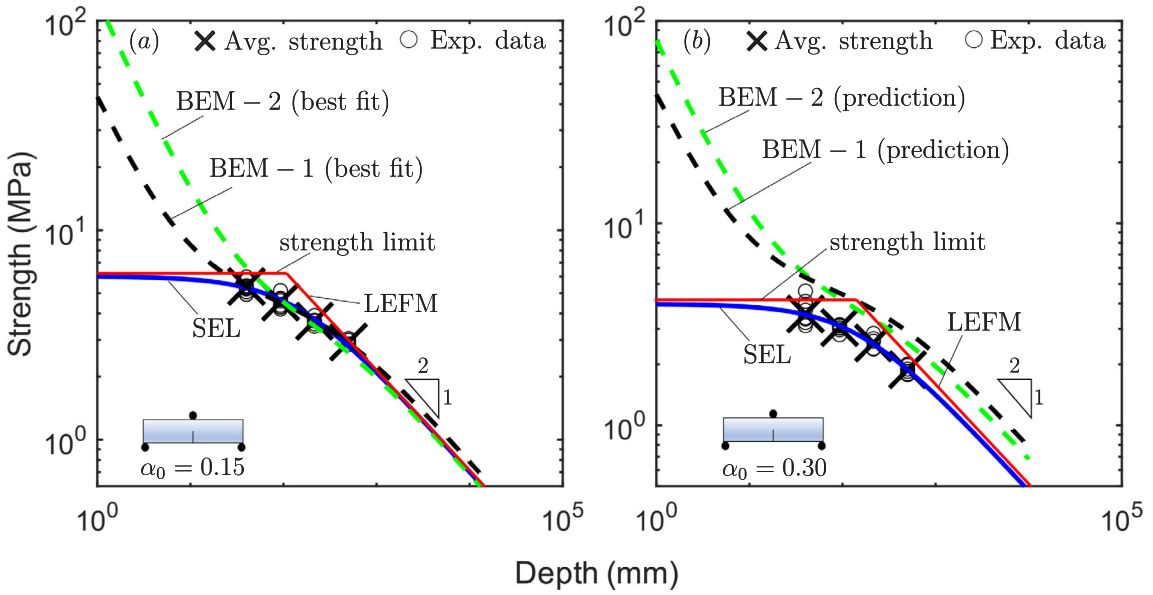

Fig. 11. Optimum fit of Hoover et al. test data [41,42] by SEL and BEM for (a) $\alpha_0 = 0.15$ and (b) $\alpha_0 = 0.3$.

predict the structural strength for the case $\alpha_0 = 0.3$ (Fig. 11b).

The optimal fitting by SEL resulted into an estimated fracture toughness $K_{IC} = 1.49$ MPa m$^{1/2}$ and an effective crack $c_f = 21.0$ mm [42]. Exploiting the link between c_f and material strength proposed by Cusatis and Schauffert [61] and the subsequent refinement proposed by Yu et al. [39], the material tensile strength calculated from SEL is $f_t = K_{Ic}\sqrt{0.29/c_f} = 5.23$ MPa. Fig. 11b shows the size effect predicted by SEL leveraging the foregoing results and recalculating the dimensionless energy release functions $g(\alpha)$ and $g'(\alpha)$ for $\alpha_0 = 0.3$. The CoV of errors of fit (normalized by data mean) provided by the best fit through SEL is 4.15% and 2.31% for $\alpha_0 = 0.15$ and $\alpha_0 = a_0/D = 0.30$, respectively.

As seen in the figures, not only the Type 2 SEL is in excellent agreement with the experimental data but also the asymptotic behavior for both small and large sizes follows the existing, extensively validated, physical models. For large sizes, the SEL converges asymptotically to the LEFM whereas, for small enough sizes, the structural strength tends to the strength limit. It is important to stress here again that the curve shown in Fig. 11b, which is in excellent agreement with the experimental data, is *a prediction* made by the SEL, with the main parameters calibrated against another set of data.

The BEM, in contrast, is characterized by a completely different asymptotic behavior, especially for small beam sizes. This is very clear from Fig. 11a and b each featuring the following cases: (1) BEM – 1: best fitting obtained by jointly optimizing K_{Ic}, f_t and β, and (2) BEM – 2: best fitting obtained by fixing $K_{Ic} = 1.49$ MPa m$^{1/2}$ and $f_t = 5.59$ MPa according to [37] and optimizing β. As can be noted, for both $\alpha_0 = 0.15$ (best fitting) and $\alpha_0 = 0.30$ (prediction), BEM provides an excessive, unrealistically high, structural strength, which increases (at the unreasonable slope of $1/D$) in the small size range.

A consequence of the wrong asymptotics in BEM is that its predictions are strongly affected by the value chosen for the parameter β. To give an example, the best fits shown in Fig. 11a provided $\beta = 0.11$, $K_{Ic} = 1.61$ MPa m$^{1/2}$ $f_t = 7.40$ MPa with a CoV of 0.91% and $\beta = 0.61$, $K_{Ic} = 1.49$ MPa m$^{1/2}$ $f_t = 5.59$ MPa with a CoV of 7.93%, respectively. However, with the same fitting parameters, the prediction for the case $\alpha_0 = 0.30$ was rather inaccurate. Both fittings exhibited a CoV of 50.24% and 45.69 %, respectively, despite the limited data range.

Of course, the agreement between BEM and the experimental data can be improved by including the data for all the notch lengths in the calibration of the parameters, as proposed in [37]. However, the fact that a decent agreement could be achieved in such a case does not imply a predictive ability of the BEM. In contrast, the very poor prediction obtained by calibrating the BEM using a subset of the experimental data (Fig. 11a and b) inevitably shows the importance of capturing the asymptotic behavior and gives another reason for doubting the applicability of BEM in structural design. Further comparisons between SEL and BEM, with related discussions, can be found in [39,40].

6. Conclusions

1. The BEM is not based on the cohesive crack model and violates its asymptotic properties. The structure of the BEM does not even allow asymptotic matching of cohesive crack model properties.
2. Although the maximum aggregate size, d_m, affects the properties of the cohesive crack model, the intuitive way by which the effect of d_m is introduced in the latest version of the BEM gives an incorrect small-size asymptote of the size effect curve.
3. Because of the ambiguity in defining the required stress profile over the ligament, the BEM cannot be applied to specimens or structures other than the standard mode I fracture specimens.

4. The stress distribution across the ligament is not calculated but assumed, and conflicts with what is obtained from the cohesive crack model.
5. Comparisons with the test data on size effect reveal extensive disagreements. Especially, the optimum fit by the BEM grossly deviates from the results of most extensive series of tests conducted so far—Hoover et al.'s tests of notched beams with a very broad range of size and notch depths. In particular, it is shown that when BEM is used as a predictive theory, the CoV of errors of fit can be significant, in the order of 50%. In contrast, the predictions of SEL are always in excellent agreement, with a CoV in the order of 4 %.
6. The BEM does not properly distinguish between Type 1 and 2 size effects.
7. Since it does not include any description of the randomness of the material strength, the BEM cannot capture the statistical size effect.
8. Although the proximity of a boundary does influence the fracture behavior, this influence is more complex than considered in the BEM and cannot be reduced to a simple principle. But the cohesive crack band model with a finite RVE automatically captures this influence.
9. Because of the aforementioned problems, the BEM, unlike the SEL, is not applicable to structural design, is not relevant to developing the design code provisions for size effects on structural strength, cannot be used as the basis for measuring the fracture energy, and is not transplantable to other quasibrittle materials.
10. The foregoing conclusions and the BEM critique are important for all quasibrittle materials, especially aircraft fiber composites, tough ceramics, sea ice, large landslides, rock, stiff soils, micrometer-scale devices, bone and other biomaterials, and biomimetics, for all of which the non-statistical size effect has yet to become properly recognized in design and engineering practice.

Acknowledgments

CC would like to acknowledge the start up fund provided by Case Western Reserve University, which was partially used to support this research. MS acknowledges the financial support from the Haythornthwaite Foundation through the ASME Haythornthwaite Young Investigator Award. JL thanks NSF for partial support under grant CMMI- 1361868 to the University of Minnesota. CGH thanks Arizona State University and the Ira A. Fulton Schools of Engineering for providing research startup funds to conduct this research. ZPB thanks ARO for partial support under grant W911NF-19-1-0039 to Northwestern University. Discussions in ACI Committee 446, Fracture Mechanics, under the current chair CC and past chair CG, were particularly helpful.

Appendix A. General derivation of SEL from energy conservation and dimensional analysis

The release of complementary strain energy Π engendered by fracture is a function of: (1) the length a of the fracture (or of crack band) at maximum load, and (2) the area of the zone damaged by fracturing, which is $w_c a$, where $w_c = nd_m$ = material constant = width of crack band swept by fracture process zone width during propagation of the main crack, d_m = maximum aggregate size, and n = 2 to 3. According to Buckingham theorem of dimensional analysis, Π must be expressed as a function of dimensionless parameters, which may be taken as $\alpha_1 = a/D$ and $\alpha_2 = w_c a/D^2$. Then

$$\Pi = \frac{1}{2E}\left(\frac{P}{bD}\right)^2 bD^2 f(\alpha_1, \alpha_2) \tag{32}$$

For geometrically similar structures of different sizes, f must be a smooth function independent of D. The energy conservation during crack growth necessitates that $\partial\Pi/\partial a = G_f b$, where G_f = critical value of energy release rate. Noting that

$$\frac{\partial f}{\partial a} = \frac{\partial f}{\partial \alpha_1}\frac{\partial \alpha_1}{\partial a} + \frac{\partial f}{\partial \alpha_2}\frac{\partial \alpha_2}{\partial a} \tag{33}$$

where $\partial\alpha_1/\partial a = 1/D$ and $\partial\alpha_2/\partial a = w_c/D^2$, we consider the first two linear terms of a Taylor series expansion, $f(\alpha_1, \alpha_2) \approx f(0, 0) + f_1\alpha_1 + f_2\alpha_2$, where $f_1 = \partial f/\partial\alpha_1$, $f_2 = \partial f/\partial\alpha_2$. Setting $P = b\mathrm{d}\sigma$, we obtain

$$\left(\frac{f_1}{D} + \frac{f_2 w_c}{D^2}\right)\frac{P^2}{2bE} = G_f b \tag{34}$$

Rearranging, setting $P = bD\sigma_{Nc}$, and solving the foregoing equation for σ_{Nc} (nominal strength of structure), we obtain from Eq. (34) the deterministic (or energetic) size effect in Eq. (5), in which $D_0 = w_c f_2/f_1$ = constant (independent of size D), and $Bf_t = \sqrt{2G_f E/f_2 w_c}$. Note that this derivation rests only on the energy conservation principle and on the hypothesis that the size, w_c (width or length), of the fracture process zone at the front of dominant crack is a constant (a material property). Only geometrically similar structures are considered, and a is assumed to be non-zero, which means Type 2 size effect.

References

[1] Bažant ZP. Size effect in blunt fracture: concrete, rock, metal. J Eng Mech 1984;110:518–35.
[2] Bažant ZP, Kim JK. Size effect in shear failure of longitudinally reinforced beams. J Am Concr Inst 1984;81:456–68.
[3] Leonhardt F, Walther R, Dilger W. Shear tests on continuous beams. Deutscher Ausschuss für Stahlbeton 1964;163:138.

[4] Kani GNJ. How safe are our large reinforced concrete beams. ACI J 1967;64:128–41.
[5] Iguro M, Shioiya T, Nojiri Y, Akuyama H. Experimental studies on shear strength of large reinforced conrete beams under uniformly distributed load. Concr Lib Int (Jpn Soc Civil Eng) 1985;5:137–54. (transl. from JSCE 1984).
[6] Rüsch H, Hilsdorf H. Deformation Characteristics of Concrete Under Axial Tension. Voruntersuchungen Bericht (preliminary report); 1963, Report No. 44.
[7] Hughes BP, Chapman GP. The complete stress-strain curve for concrete in direct tension. RILEM Bull (Paris) 1966;30:95–7.
[8] Evans RH, Marathe MS. Microcracking and stress-strain curves in concrete for tension. Mater Struct 1968;1:61–4.
[9] Weibull W. Phenomenon of rupture in solids. Proc Roy Swedish Inst Eng Res (Ingenioersvetenskaps Akad. Hand.) 1939;53:1–55.
[10] Weibull W. A statistical theory of strength of materials. Ingvetensk Akad Handl 1939;151:5–45.
[11] Weibull W. A statistical distribution function of wide applicability. J Appl Mech 1951;103:293–7.
[12] Bažant ZP, Le JL. Probabilistic mechanics of quasibrittle structures: strength, lifetime, and size effect. Cambridge University Press; 2017.
[13] Subcommitee on English Version of Standard Specifications for Concrete Structures. JSCE Guidelines for Concrete No. 15: Design. Japan Society of Civil Engineering; 2007.
[14] Bažant ZP, Yavari A. Is the cause of size effect on structural strength fractal or energetic–statistical? Eng Fract Mech 2005;72:1–31.
[15] Bažant ZP, Yavari A. Response to A. Carpinteri, B. Chiaia, P. Cornetti and S. Puzzi's comments on 'Is the cause of size effect on structural strength fractal or energetic-statistical?'. Eng Fract Mech 2007;74:2897–910.
[16] Fédération Internationale du Béton (fib): Model Code 2010, final draft, vol. 1, Bulletin 65, and, vol. 2, Bulletin 66, Lausanne, Switzerland; 2012.
[17] Muttoni A, Schwartz J. Behavior of beams and punching in slabs without shear reinforcement. In: IABSE colloquium (No. CONF). IABSE Colloquium. Vol. 62; 1991.
[18] Collins MP, Kuchma D. How safe are our large, lightly reinforced concrete beams, slabs, and footings? Struct J 1999;96:482–90.
[19] Swiss Society of Engineers and Architects, SIA Code 262 for Concrete Structures, Zürich, Switzerland; 2003. 94p.
[20] Bažant ZP, Yu Q. Designing against size effect on shear strength of reinforced concrete beams without stirrups: II. Verification and calibration. J Struct Eng ASCE 2005;131:1885–97.
[21] Bentz EC, Collins MP. Development of the 2004 Canadian Standards Association (CSA) A23. 3 shear provisions for reinforced concrete. Can J Civil Eng 2006;33:521–34.
[22] Bentz EC, Vecchio FJ, Collins MP. Simplified modified compression field theory for calculating shear strength of reinforced concrete elements. ACI Mater J 2006;103:614–24.
[23] Muttoni A, Fernandez Ruiz M. Shear strength of members without transverse reinforcement as function of critical shear crack width. ACI Struct J 2008;105:163–72.
[24] Muttoni A, Ruiz MF, Bentz E, Foster S, Sigrist V. Background to fib Model Code 2010 shear provisions. Part II: punching shear. Struct Concr 2013;14:204–14.
[25] Sigrist V, Bentz E, Ruiz MF, Foster S, Muttoni A. Background to the fib Model Code 2010 shear provisions. Part I: Beams and slabs. Struct Concr 2013;14:195–203.
[26] Ruiz MF, Muttoni A, Sagaseta J. Shear strength of concrete members without transverse reinforcement: a mechanical approach to consistently account for size and strain effects. Eng Struct 2015;99:360–72.
[27] Yu Qiang, Le Jia-Liang, Hubler HH, Wendner R, Cusatis G, Bažant ZP. Comparison of main models for size effect on shear strength of reinforced and prestressed concrete beams. Struct Concr (fib) 2016;17:778–89. https://doi.org/10.1002/suco.201500126.
[28] Dönmez A, Bažant ZP. Size effect on punching strength of reinforced concrete slabs with and without shear reinforcement. ACI Struct J 2017;114:875–86.
[29] Fernandez Ruiz M, Muttoni A. Size effect in shear and punching shear failures of concrete members without transverse reinforcement: differences between statically determinate members and redundant structures. Struct Concr 2018;19:65–75.
[30] Dönmez A, Bažant ZP. Critique of Critical Shear Crack Theory (CSCT) for *fib* Model Code articles on shear strength and size effect of reinforced concrete beams. Struct Concr 2019;20:1–14. (based on SEGIM Report No. 18-10/788c, Northwestern University, 2018; posted on arXiv: <1810.11506>).
[31] Hu X, Wittmann F. Size effect on toughness induced by crack close to free surface. Eng Fract Mech 2000;65:209–21.
[32] Banerjee PK, Butterfield R. Boundary element methods in engineering science. New York: McGraw-Hill; 1981.
[33] Duan K, Hu X, Wittmann FH. Boundary effect on concrete fracture and non-constant fracture energy distribution. Eng Fract Mech 2003;70:2257–68.
[34] Duan K, Hu X, Wittmann FH. Scaling of quasi-brittle fracture: boundary and size effect. Mech Mater 2006;38:128–41.
[35] Hu X, Duan K. Size effect and quasi-brittle fracture: the role of FPZ. Int J Fracture 2008;154:3–14.
[36] Hu X, Duan K. Mechanism behind the size effect phenomenon. J Eng Mech 2010;136:60–8.
[37] Hu X, Guan J, Wang Y, Keating A, Yang S. Comparison of boundary and size effect models based on new developments. Eng Fract Mech 2017;175:146–67.
[38] Hoover CG, Bažant ZP. Universal size-shape effect law based on comprehensive concrete fracture tests. J Eng Mech 2014;140:473–9.
[39] Yu Q, Le JL, Hoover CG, Bažant ZP. Problems with Hu-Duan boundary effect model and its comparison to size-shape effect law for quasi-brittle fracture. J Eng Mech 2009;136:40–50.
[40] Hoover CG, Bažant ZP. Comparison of the Hu-Duan boundary effect model with the size-shape effect law for quasi-brittle fracture based on new comprehensive fracture tests. J Eng Mech 2014;140:480–6.
[41] Hoover CG, Bažant ZP, Vorel J, Wendner R, Hubler MH. Comprehensive concrete fracture tests: description and results. Eng Fract Mech 2013;114:92–103.
[42] Hoover CG, Bažant ZP. Comprehensive concrete fracture tests: size effects of types 1 & 2, crack length effect and postpeak. Eng Fract Mech 2013;110:281–9.
[43] Hoover CG, Bažant ZP. Cohesive crack, size effect, crack band and work-of-fracture models compared to comprehensive concrete fracture tests. Int J Fracture 2014;187:133–43.
[44] Caglar Y, Sener S. Size effect tests of different notch depth specimens with support rotation measurements. Eng Fract Mech 2016;157:43–55.
[45] Bažant ZP, Pfeiffer PA. Determination of fracture energy from size effect and brittleness number. ACI Mater J 1987;84:463–80.
[46] Bažant ZP, Kazemi MT. Determination of fracture energy, process zone length and brittleness number from size effect, with application to rock and concrete. Int J Fracture 1990;44:111–31.
[47] Bažant ZP, Kazemi MT. Size effect in fracture of ceramics and its use to determine fracture energy and effective process zone length. J Am Ceram Soc 1990;73:1841–53.
[48] Bažant ZP, Daniel IM, Li Z. Size effect and fracture characteristics of composite laminates. J Eng Mater 1996;118:317–24.
[49] Bažant ZP. Scaling of quasibrittle fracture: asymptotic analysis. Int J Fracture 1997;83:19–40.
[50] Bažant ZP, Planas J. Fracture and size effect in concrete and other quasibrittle materials. Boca Raton: CRC Press; 1998.
[51] Bažant ZP. Scaling theory for quasibrittle structural failure. Proc Natl Acad Sci USA 2004;101:13400–7.
[52] Carloni C, Santandrea M, Baietti G. Influence of the width of the specimen on the fracture response of concrete notched beams. Eng Fract Mech, in press, doi:https://doi.org/10.1016/j.engfracmech.2018.04.045.
[53] Bažant ZP, Novák D. Probabilistic nonlocal theory for quasibrittle fracture initiation and size effect. I: Theory. J Eng Mech 2000;126:166–74.
[54] Bažant ZP, Novák D. Probabilistic nonlocal theory for quasibrittle fracture initiation and size effect. II: Application. J Eng Mech 2000;126:175–85.
[55] Bažant ZP. Concrete fracture models: testing and practice. Eng Fract Mech 2002;69:165–205.
[56] Bažant ZP, Pang SD. Mechanics-based statistics of failure risk of quasibrittle structures and size effect on safety factors. Proc Natl Acad Sci USA 2006;103:9434–9.
[57] Bažant ZP, Vořechovský M, Novák D. Asymptotic prediction of energetic-statistical size effect from deterministic finite-element solutions. Journal of engineering mechanics. J Eng Mech 2007;133:153–62.
[58] Cusatis G, Cedolin L. Two-scale study of concrete fracturing behavior. Eng Fract Mech 2007;74:3–17.
[59] Cedolin L, Cusatis G. Identification of concrete fracture parameters through size effect experiments. Cem Concr Comp 2008;30:788–97.
[60] Pang SD, Bažant ZP, Le JL. Statistics of strength of ceramics: finite weakest-link model and necessity of zero threshold. Int J Fracture 2008;154:131–45.
[61] Cusatis G, Schauffert EA. Cohesive crack analysis of size effect. Eng Fract Mech 2009;76:2163–73.
[62] Bažant ZP, Le JL, Bažant MZ. Scaling of strength and lifetime probability distributions of quasibrittle structures based on atomistic fracture mechanics. Proc Natl

Acad Sci USA 2009;106:11484–9.
[63] Le JL, Bažant ZP, Bažant MZ. Unified nano-mechanics based probabilistic theory of quasibrittle and brittle structures: I. Strength, static crack growth, lifetime and scaling. J Mech Phys Solids 2011;59:1291–321.
[64] Le JL, Falchetto AC, Marasteanu MO. Determination of strength distribution of quasibrittle structures from mean size effect analysis. Mech Mater 2013;66:79–87.
[65] Salviato M, Kirane K, Ashari SE, Bažant ZP, Cusatis G. Experimental and numerical investigation of intra-laminar energy dissipation and size effect in two-dimensional textile composites. Compos Sci Tech 2016;135:67–75.
[66] Salviato M, Chau VT, Li W, Bažant ZP, Cusatis G. Direct testing of gradual postpeak softening of fracture specimens of fiber composites stabilized by enhanced grip stiffness and mass. J Appl Mech 2016;83:111003.
[67] Salviato M, Ashari SE, Cusatis G. Spectral stiffness microplane model for damage and fracture of textile composites. Compos Struct 2016;137:170–84.
[68] Kirane K, Salviato M, Bažant ZP. Microplane-triad model for elastic and fracturing behavior of woven composites. J Appl Mech 2016;83:041006.
[69] Mefford CH, Qiao Y, Salviato M. Failure behavior and scaling of graphene nanocomposites. Compos Struct 2017;176:961–72.
[70] Qiao Y, Salviato M. Study of the fracturing behavior of thermoset polymer nanocomposites via cohesive zone modeling. Compos Struct 2019;220:127–47.
[71] Qiao Y, Salviato M. Strength and cohesive behavior of thermoset polymers at the microscale: a size-effect study. Eng Fract Mech 2019;213:100–17.
[72] Ko S, Yang J, Tuttle ME, Salviato M. Fracturing behavior and size effect of discontinuous fiber composite structures with different platelet sizes. arXiv preprint, arXiv:<1812.08312>.
[73] Li W, Jin Z, Cusatis G. Size effect analysis for the characterization of marcellus shale quasi-brittle fracture properties. Rock Mech Rock Eng 2018:1–18.
[74] Bažant ZP, Novák D. Energetic-statistical size effect in quasibrittle failure at crack initiation. ACI Mater J 2000;97:381–92.
[75] Irwin GR. Fracture. Handbuch der Physik vol. 6. Berlin: Springer; 1958.
[76] Murakami Y. The stress intensity factor handbook. Pergamon Press; 1987.
[77] Paris PC, Tada H. The stress analysis of cracks handbook. New York, NY, 10016: American Society of Mechanical Engineers; 2000.
[78] Bažant ZP. Scaling of structural strength. Elsevier; 2005.
[79] Petch NJ. The cleavage strength of polycrystals. J Iron Steel Inst 1954;174:25–8.
[80] Griffith AA. The phenomena of rupture and flow in solids. Phil Trans R Soc Lond A 1921;221:163–98.
[81] Orowan E. Fracture and strength of solids. Rep Prog Phys 1949;12:185–232.
[82] Sanford RJ. Principles of fracture mechanics. New Jersey: Prentice Hall; 2003.
[83] Gdoutos EE. Fracture mechanics: an introduction. Berlin: Springer; 2006.
[84] Zehnder A. Fracture mechanics. Berlin: Springer; 2012.
[85] Anderson TL. Fracture mechanics: fundamentals and applications. CRC Press; 2017.
[86] Bažant, Li Z. Modulus of rupture: size effect due to fracture initiation in boundary layer. J Struct Eng 1995;121:739–46.
[87] Levenberg K. A method for the solution of certain non-linear problems in least squares. Q Appl Math 1944;2:164–8.
[88] Marquardt DW. An algorithm for least-squares estimation of nonlinear parameters. SIAM J Appl Math 1963;11:431–41.
[89] Dassault Systemes ABAQUS Documentation, Providence, RI; 2016.
[90] Bazant ZP, Yu Q, Gerstle W, Hanson J, Ju JW. Justification of ACI-446 proposal for updating ACI code provisions for shear design of reinforced concrete beams. ACI Struct J 2007;104(5):601–10. (with Errata—title correction, Nov.-Dec., p. 767).